On the Non Development of an Intense African Easterly Wave; Observations and Predictability

Alan Brammer * and Chris D. Thorncroft

Department of Atmospheric And Environmental Science, University at Albany, State University of New York, Albany, New York

**Corresponding author address:* Alan Brammer, University at Albany, State University of New York, 1400 Washington Ave., Albany, NY 12222

E-mail: abrammer@albany.edu

ABSTRACT

A strong African easterly wave (AEW) left the west African coast in early September 2014, global numerical and operational forecasts suggested a potential for tropical cyclogenesis once the AEW was over the eastern Atlantic. A large region of dry air was also present to the north of the disturbance. During this time the Hurricane Severe Storm Sentinel field campaign was making observations of tropical cyclones with an unmanned global hawk aircraft. This enabled observations of the AEW over the eastern Atlantic during its time of potential development and during the time of interaction with the encroaching dry air. Analysis and observations show that after leaving the coast, the synoptic scale vortex was not well aligned vertically and entrained air above and below the main jet-level vortex. Dropsonde observations highlight the dry air undercutting the mid-level recirculation region on the southwestern corner. This entrainment of dry air constrains precipitation within the trough and the vortex decays as the column continues to be displaced horizontally and lose vertical alignment allowing for further entrainment of dry air above and below. Ensemble sensitivity analysis identifies a consistent impact of the moisture on the western side of the disturbance for precipitation occurring within the trough. A consistent bias in the forecasts is observed through an over-intensification of the vortex in the first 24–48 hours of the forecast, providing more favourable conditions for precipitation around the vortex and thus a positive feedback loop is initiated.

1. Introduction

Synoptic scale westward propagating disturbances from over West Africa and the eastern Atlantic have been associated with Tropical Cyclogenesis for over a century (Piersig 1944). On rare occasions, these disturbances have intensified over West Africa to a point where they are almost tropical storm strength while still over land and rapidly develop over the eastern Atlantic given the surface moisture flux (Erickson 1963). Further analysis has revealed a strong link between these westward propagating African disturbances and tropical cyclone activity across most of the main development region of the Atlantic; accounting for roughly half of the Atlantic tropical cyclones (e.g. Carlson 1969a,b; Frank 1970; Landsea 1993). Burpee (1972, 1974) showed that these westward propagating disturbances were waves with a periodicity of 3–5 days, approximate wavelength of around 2500 km and a peak vortex around the level of the African easterly jet around 700–600 hPa with a cold-core low-level structure.

Tropical cyclogenesis has been associated with a few necessary large-scale conditions associated with a pre-existing low-level disturbance, Gray (1968) showed that genesis was more likely given warm SSTs ($\geq 26.5°$C), increased low-level moisture around the disturbance and relatively low-shear. These conditions favor the maintenance of deep convection associated with the tropical cyclogenesis process. For genesis events over the eastern Atlantic, (Bracken and Bosart 2000) highlighted there was an upper-tropospheric ridge poleward of the disturbance which was associated with large-scale ascent around the disturbance. The tropical easterly jet along the equator also favors an upper-level anticyclone near the West African coast creating a localized region of low deep-layer vertical wind shear and favorable conditions for deep convection (McBride and Zehr 1981). Deep convection and the associated potential vorticity generation over the coastal region has been shown to be a crucial stage for AEWs for both genesis events (Berry and Thorncroft

2005). Multiple factors can be attributed to influencing deep convection around the coastal region and can therefore be linked to genesis over the eastern Atlantic. (e.g. Ventrice et al. 2012; Chiao and Jenkins 2010)

Analysis of developing and non-developing AEWs has revealed further differences for why a few AEWs are able to support tropical cyclogenesis events. Hopsch et al. (2010) showed that developing troughs already had stronger low-level vorticity and increased ascent over the coastal region prior to leaving the continent. The ability for deep convection to be sustained as the troughs leave the coast is important for maintaining and continuing the intensification of the vortex (Arnault and Roux 2009, 2010), though at this point in the genesis cycle the coverage of deep convection can be more important than the intensity (Leppert II et al. 2013b,a). Berry and Thorncroft (2005) proposed that the generation as well as merging of PV anomalies over the coastal region was a crucial stage in the lifecycle of an AEW.

The modulation of the synoptic scale characteristics by the AEW are especially important for convective activity over the eastern Atlantic given the presence of dry air north of the AEJ, either of Saharan origin or subsidence from the sub-tropics of mid-latitudes (Dunion and Velden 2004; Braun 2010). AEW troughs are characterised by a propagating region of increased moisture and vorticity, in a Lagrangian reference a strong circulation around the trough can potentially provide protected region of favourable conditions for convection and intensification (Dunkerton et al. 2009). However, AEWs over West Africa are typically cold-core at low-levels developing low-level vorticity as they leave the coast and transition into the oceanic environment (Janiga and Thorncroft 2012). Therefore regions of closed circulation at the level of the AEJ will likely not have closed circulation above or below vortex has continued to intensify (Wang and Hankes 2014). Therefore interactions between the trough and surrounding environment have been shown to be not only possible but also important for convective activity near the coastal region. Strengthening MCSs leaving the coast were associated with increased southerly moisture flux associated with the downstream wave (Dieng et al. 2014). Similarly, differences in low-level moisture downstream (north-west) of strong AEW troughs was a significant factor in the composite analysis of developing and non-developing waves (Brammer and Thorncroft 2015). While Fritz and Wang (2013) showed that mid-level dry air intrusions were associated with suppressed convection and halting the intensification of an otherwise favourable system.

Ensemble numerical simulations of tropical cyclogenesis cases have also highlighted the impact of variability in the moisture field around pre-genesis disturbance. Variability in the initial conditions of moisture, convective available potential energy (CAPE) around the trough or vortex strength can affect the short term spin-up of the vortex, creating large ensemble spread that then continues to amplify through the forecast (Torn and Cook 2013). Ensemble-based sensitivity analysis for forecasts of AEW and genesis from AEWs have shown in specific cases the correlation between moisture west and north of the trough in the initial conditions to forecast intensity (Torn 2010; Rios-Berrios et al. 2016). These sensitivities to not only initial vortex charactersitics but also synoptic scale environmental characteristics highlight the potential difficulties for operational numerical forecasts of tropical cyclogenesis. Komaromi and Majumdar (2015) showed that about 50% of cases genesis forecasts were related to the predicted favourability of the environment, while the remainder of cases are most sensitive to the strength and location of the disturbance. It is therefore not surprising that deterministic forecasts from various global models have relatively high false alarm rates for tropical cyclogenesis over the Eastern Atlantic (Halperin et al. 2013).

In 2014 the NASA Hurricane Severe Storm Sentinel (HS3) field campaign were observing tropical systems with an unmanned high-altitude (18 km; 50 hPa) aircraft (Braun et al. 2016). This aircraft had a 24 hr flight time and therefore allowed for in-situ observations of AEW troughs as far east as around 30°W. Given the uncertainty regarding the influence of SAL or dry air on developing disturbances this platform provided a unique opportunity to observe potential cyclogenesis events over the eastern Atlantic. This paper documents the evolution and forecasts of a non-developing system that was officially designated as invest AL90 during the first week of September 2014. While previous research has compared ensemble forecasts for developing cases or provided analysis for developing and non-developing cases, there are limited results regarding the evolution and predictability of strong non-developing cases.

A synoptic overview of the AEW trough associated with AL90 will be presented in section 3, this analysis will discuss the observations and reanalysis structure of the trough and embedded disturbance. Section 4 will then include an analysis of the ensemble forecasts of the disturbance and it's forecasts tropical cyclogenesis over the eastern Atlantic. A discussion of the observed evolution in contrast to the numerical simulations will follow in section 5

2. Data & Methodology

Climate Forecast System (CFS) version 2 data was used for the analysis of the evolution of the AEW trough and for verification against the ensemble forecasts. The will be used, with climatological values calculated with respect to the CFS Reanalysis (CFSR) for the period of 1979-2010 (Saha et al. 2010, 2014). Observations from the HS3 global hawk platform include dropsondes (measuring Temperature, Relative Humidity and wind) as well as a cloud physics lidar (CPL) which is able to detect multiple layers or aerosol throughout the troposphere. Dropsondes were post-processed through Aspen Wang et al. (2010) and reprocessed to correct for an upper-level dry bias (Young 2016). Observed precipitation rates are obtained from the Tropical Rainfall Measuring Mission (TRMM) Multisatellite Precipitation Analysis (TRMM product 3B42; Huffman et al.

2007). Ensemble forecasts are analysed from the operational NCEP Global Ensemble Forecast System (GEFS) archived at NOAA NCEI website.

The AEW trough is tracked objectively utilising a multiple variable tracker similar to the NCEP tropical cyclone tracker (Marchok 2002). The AEW trough is tracked through a combination curvature vorticity at 850, 700 and 500 hPa, geopotential height at 850 hPa and relative vorticity 850 and 700 hPa. Tracking both relative and curvature vorticity at multiple levels enables a smooth and continuous track across of the circulation associated with the trough and later the incipient vortex. Propagation of the disturbance is calculated as a combination of extrapolation of the previous phase speed and axis-symmetric steering flow calculated over 850-400 hPa over a radius of 400 km around the disturbance. Ensemble forecast tracks follow the same tracking critera using the analysis position as the initial estimated location for each 0000 UTC initialisation time. Analysis locations are then re-centered in each ensemble to account for the perturbations in the initial conditions.

3. AEW Synoptic History

a. Synoptic Evolution

The invest 90L in September 2014 spawned within the trough of a well defined African easterly wave (AEW), the vortex signature of which can be traced back to over Ethiopia on August 27th (not shown). While the AEW trough transitioned across Central and Western Africa there were continuous deep convective bursts and accumulated precipitation of over 15 mm across large areas of the Sahel (Fig. 1). Though as the trough left the west African coast on September 4th, associated precipitation rapidly declined over the eastern Atlantic, with only a small area of deep convection and precipitation occurring on the northern side of the vortex during September 6th-7th. This period of reduced convective activity coincides with the trough transitioning into the anomalously dry environment over the eastern Atlantic, where TPW anomalies were more than 10 mm below normal.

As the trough left the West African Coast, the National Hurricane Center (NHC) declared the system as invest AL90 (90L). The official five-day genesis forecast peaked for 90L with a 40% chance of tropical cyclogenesis for the 09/04 1800UTC forecast. Given the wave's history across the African continent and the global model forecasts at the time this invest was also of interest to the NASA Hurricane and Severe Storm Sentinel (HS3) field program which deployed the Global Hawk observing platform and made in-situ observations of the system between 09/05 1800UTC and 09/06 0400UTC.

The accumulated precipitation in figure 1 shows the trough had regular convection within 750 km of the jet-level circulation across the Sahel. A vortex centric time-series of precipitation, with relative vorticity and the surrounding (300-750 km) 850 hPa specific humidity, highlights this evolution also showing that the trough is associated with a significant diurnal cycle in precipitation while over land (Fig. 3). The 3 hr precipitation time series show consistent evening peak for the days between 08/28 to 09/03 within only one exception on the evening of 08/31. The time-series of vorticity and humidity during this continental stage show that both humidity and vorticity remain relatively stable until the trough reaches the coast.

Figure 2 displays the vertical structure of the vorticity around the trough and specific humidity profile for the same time period. During the trough's continental transit, the vortex shows the typical jet-level maximum with a cold-core dynamical signature below, as the trough transits over the coastal region the vorticity around the trough increases at low-levels slightly. This pattern matches the climatological pattern shown by Janiga and Thorncroft (2012). It is worth noting though that

Janiga and Thorncroft (2012) showed that the CFSR exhibited stronger low-level vorticity compared to ERA-I and TRMM heating profiles.

As the trough reaches the coast the averaged environmental humidity drops abruptly from 12 g kg^{-1} to 10 g kg^{-1} (Fig. 3), this is also representative of the large scale environment as shown by the anomalous total precipitable water field in Fig. 1. After leaving the coast the precipitation remains relatively weak and the vorticity associated with the trough slowly weakens. The NASA HS3 flight sampled the system after the peak intensity, as the vortex began to slowly weaken during the evening of 09/05 (represented by the shaded background in Fig. 3).

The interaction of the vortex with the environmental dry air is shown with vertical cross sections for three times in Fig. 4. As the trough leaves the coast on 09/04, the vortex has strong relative vorticity extending between 850 hPa up to 500-400 hPa. Low-level positive (blue) specific humidity anomalies extend throughout the lower troposphere within the vortex with an extension to the west at very low-levels (Fig. 4a). Farther west from the trough is the very dry environment over the eastern Atlantic, with anomalies below -6 g kg^{-1} between 25°W to 40°W and below 700 hPa.

By 1200UTC on September 5th, a very strong moisture gradient has developed along the western edge of the AEW vortex (Fig. 4b). The low-level extension of positive moisture anomalies has been degraded and the vortex has started to show signs of weakening. Above 550 hPa the vorticity within the cross section has been reduced to below 3x10^{-5} s^{-1} and the time-series of 850 hPa circulation also shows that at this time the low-level vorticity has started to weaken. Eighteen hours later (Fig. 4c), the vortex has continued to weaken although the moisture gradient along the western edge remains strong at approximately 16 g kg^{-1} over a 500 km range. The vortex has continued to become less organized and negative moisture anomalies now exist below the jet-level vortex on the western edge of the trough.

Figure 5 shows the evolution of the equivalent potential temperature (θ_e) and wave relative circulation at the same three times as shown in Fig. 4. At 1800UTC on 09/04 the is around 20°W with the mid-level vortex slightly south-west of the lower-level vortex (Figure 5c,f). Precipitation associated with the trough is colocated with the closed circulation at 500 hPa but on the western edge of the circulation at 850 hPa. θ_e at both levels exceeds 336 K within region of closed circulation, though outside of the circulation low θ_e ($\leq$ 330 K) can be seen wrapping around the western and southern flanks at both levels. By 1200 UTC on September 5th the north-south elongated mid-level circulation, has rotated cyclonically to have a NE-SW alignment with low θ_e on all sides except the north-east. A NW-SE tilt is still present in the vertical with the low-level circulation at this time still over Cape Verde. This vertical tilt continues and is very apparent by 0600 on September 6th as the mid-level circulation remains SW of the low-level vortex.

Precipitation associated with the trough on 09/06 is situated near the center of the low-level circulation around 15°N and 30°W. This precipitation however is on the outer boundary of the 500 hPa circulation, which is offset approximately 250 km to the SW. Although there remains a region of increased θ_e at 500 hPa in vertical alignment with the low-level circulation, the circulation at this level is now entraining lower θ_e from the southwest over the low-level vortex.

It is expected that the vertical tilt associated with the trough acts to feedback negatively on the evolution of the convection and associated vorticity generation. As the mid-level vortex is displaced to the west and southwest, the vortex will impose cyclonic circulation around the tilted column. Due to the weak strength and lack of organisation of the vorticity at this time, this feedback is likely slow and relatively small compared to tilted tropical cyclone evolution. The vortex associated with the AEW however shows a slow cyclonic rotation with the mid-level vortex moving W to SW of the low-level circulation. With strong horizontal gradients of moisture west of the system, this vertical tilt opens up the trough up to entraining air from the west more rapidly than a coherent vertical vortex would otherwise.

b. Characteristics of the Dry Air

The origin and characteristics of dry air over the Atlantic is typically of great interest with respect to how it impacts tropical cyclones and developing tropical cyclones. The previous discussion has shown that a large region of dry air throughout the lower troposphere was present to the west of the AEW associated with Invest 90L. Figure 6 shows the same four day evolution of the disturbance leaving West Africa with IR brightness temperature and the split-window Saharan Air Layer product from CIMSS (Dunion and Velden 2004). This product highlights the large area of dry air over the eastern Atlantic to the northwest of the convective signature and a secondary region of dry or dusty air following the trough (leaving the coast on September 6th). This product however does not specifically identify dusty air, rather it highlights dry/and or warm air at low-levels. Subjectively comparing these figures to Aerosol optical depth measured by MODIS on Terra and Aqua satellites shows that while increased AOD is present along the western edge of the circulation the large area of dry air west of the system is relatively dust free (Fig. 7). This also subjectively compares well to dust concentration in MERRA-2, which shows dust along the moisture gradient of the outer circulation but dust-free dry air over the majority of the eastern Atlantic (not shown).

This interaction between the dry air over the eastern Atlantic and the dust along the circulation periphery can also be observed in data collected by the NASA global hawk platform. Figure 9 shows a NW-SE vertical transect approaching the circulation of 90L created using both dropsonde data and aerosol layer detection from the CPL onboard. This highlights the interaction between the circulation of 90L and the low-level dry air to the west. From 21°N, 38°W to 14°N,33°W dry air is observed above from 850 hPa at the top of the boundary layer. The CPL layer detection indicates the presence of boundary layer aerosol (blue) and elevated aerosol (yellow) along the top of the boundary layer but otherwise clear air above. At 14°N, 33°W a region of increased RH and θ_e extends to west from the trough at 600 hPa. This vertical overlap of characteristics highlights the NE to SW tilted circulation discussed earlier, with the advection of drier air below the edges of the mid-level circulation. At the end of the transect, SW of the low-level circulation center, increased elevated aerosols are observed also confirming the high concentration of dust along the periphery of the circulation observed by MODIS.

4. Tropical Cyclogenesis Forecasts

The previous section has highlighted that while the AEW trough designated as invest 90L had had a convectively active history over Africa the dry air ahead of the system appeared rather unfavorable for further development over the eastern Atlantic. However, model guidance at the time was suggesting that intensification could occur at least for the short term. The National Hurricane Center issued the highest probability of genesis within 120 hrs at 40% on 09/04. This shows that the trough was viewed by the NHC forecasters and the global models as at least slightly favourable for development. Halperin et al. (2013) has shown that the GFS and other models generally have a strong false alarm bias with respect to genesis over the eastern Atlantic, so it is expected that NHC forecasters would have a lower forecast probability when compared to the global models. NHC forecast discussions briefly mention the "dry air engulfing the system" (805 PM EDT 2014/09/04) but also focus on the strong convection and "region of deep layer high moisture" around the trough axis.

This section will analyse the evolution of the forecasted developing systems compared with the verification of the non-developing system. This analysis will explore the subtleties in differences between developing and non-developing disturbances as well determining why global models can struggle with false alarms over the eastern Atlantic.

a. Operational Forecasts

The operational forecasts for each 00 UTC cycle from the Global Ensemble Forecasting System (GEFS) are shown in Fig. 10, the ensemble forecast tracks are represented by cones calculated as $\pm 1\sigma$ of across track spread around the ensemble mean. These forecast tracks highlight that, in general, the forecasts were able to capture the track of the disturbance sufficiently, with the analysis track consistently within the ensemble based cone. Although a slight poleward bias is evident for forecasts verifying on the 2nd and 3rd of September (Fig 10a). The model however consistently forecasts over intensification of the 850 hPa vortex. The time-series of the analysis vorticity and ensemble distribution of forecast vorticity shows that the analysis was weaker than 75% of the forecast ensemble members for all times after 1200UTC on September 5th.

The bias or error in the mean ensemble forecast is presented in Fig. 11 for the 4 forecasts initialised around the troughs' passage over the West African coast. While each forecast shows a slight over-intensification of the vortex around the jet-level over Africa as the troughs reach the coasts the forecast system consistently over-develops the low-level vorticity around the system. For the forecast initialised on September 4th (Fig. 11c), although there is initial over-development of the vortex over the eastern Atlantic between hours 48-72, the system has started to weaken at the later lead times. This weakening signal at later lead times becomes more evident in the subsequent forecast from Sept. 5th (Fig. 11d). This suggests that despite the early intensification of the system, the vortex is still constrained in it's longer term evolution. Related to the strength of the vortex, Fig. 12 displays a similar analysis for θ_e in the vortex. The first two forecasts initialised over the continent show a large positive bias in low-level θ_e at hours 48 and 24 respectively. The ensemble mean track at this time exhibits a poleward bias, therefore this track error likely also accounts for the thermodynamic error. Once over the ocean, all 4 forecasts show that the ensemble mean vortex had positive bias of θ_e throughout the lower troposphere compared to the analysis. Ensembles forecasts of precipitation (not shown) continued to have active convection during this time with precipitation occurring around the vortex after leaving the coast, with a notable diurnal pulse occurring in the morning hours. While TRMM 3b42 measures a similar diurnal pulse to the convection the areal average precipitation rate is about 50% of that forecast.

b. Ensemble Based Sensitivity Analysis

To understand the evolution of the forecasts and the vortex interaction with the environment, the vortex strength at each forecast hour is correlated with the vortex strength at each subsequent forecast time for the 4 initialisation times (Fig. 13). For the 09/02 ensemble forecast, there is a negative correlation between vortex strength at hours 0-18 and vortex strength at later lead times (Fig. 13a). This shows that ensembles initialised with a stronger vortex tend to end up weakening at later forecasts. At forecast hour 24, there is significant positive autocorrelation for the strength of the vortex at all subsequent hours. This is interpreted as the point at which strong ensemble members stay strong and weak members stay weaker, or that beyond this point the evolution of the system is relatively linear and a function of the vortex strength. Therefore understanding the eventual strength of the forecast is dependent on understanding the evolution of the vortex in the first 24 hours.

A similar signal in the autocorrelation of vortex strength is seen across the subsequent initialisation times. Forecasts initialised at 0000UTC 09/03 show low correlation values with respect to vortex strength over the first 36 hours, at hour 42 however a significant correlation becomes evident for the subsequent 72 hours which is consistent throughout the remaining forecast (Fig. 13b).

Once the vortex is over the ocean the autocorrelation becomes more consistent with 24-30 hour vortex strength significantly correlated with the strength of the vortex through the remaining forecast hours (Fig. 13c,d).

Figure 14 shows the correlation between precipitation within 300 km of the trough and the future strength of the vortex. Generally a similar signal is with precipitation in the first 24-48 hours showing significant correlation with vortex strength throughout the remaining forecasts. Vortex stretching through diabatic heating is likely the primary method for vorticity generation throughout this time therefore understanding the influences on the short term precipitation forecasts is crucial to understand the later evolution of the vortex. These figures highlight that the after a certain point, typically hours 24-48 for these forecasts, the vortex evolution is largely dependent on it's own strength. Members which continue to intensify have likely developed a closed circulation and are less sensitive to the surrounding environment, while weaker members may have weakened to the point where they can not re-intensify given the hostile environment to the west of the circulation.

Ensemble sensitivity analysis correlates perturbations in the analysis or short lead time variable with spread in a forecast metric at a later lead time. Sensitivity of precipitation at hour 42 with respect to lower-tropospheric moist static energy is shown in figure 15. For each of the 4 initialisation times, the 12 and 24 hour forecast moist static energy is correlated with the 42 hour precipitation. For the forecast initialised on Sept. 2nd, the main areas of sensitivity are north of the vortex, where an increase of moist static energy is related to increased precipitation or south of the disturbance where an inverse relationship is observed. The wave relative streamlines for this times, show a fairly small but also closed circulation in the lower troposphere, with strong meridional flow on the western edge. Trajectory analysis for AEWs in this region showed a similar structure with very few eastern Atlantic trajectories entrained in to the vortex while the trough was still over the continent (Brammer and Thorncroft 2017). On reaching the coastal region and leaving the continent the areas of sensitivity have shifted to the northwest and west of the vortex. The sensitivity follows the region and gradient of the dry air on the western edge as it is wrapped around the vortex. South of the vortex there is a consistent region of sensitivity with a negative correlation, showing that lower moist static energy in this region is associated with increased precipitation in the trough. A similar signal was also observed in composites of developing and non-developing AEWs in Brammer and Thorncroft (2015). This sensitivity is on a thin zonal strip of increased moist static energy, which can be seen in the analysis of θ_e in figure 5, and related to a meridional shift of this strip towards the vortex creating drier conditions on the equatorward gradient.

To summarise the previous discussion in a potentially useful realtime forecast graphic, Figure 16 shows an overview of the ensemble forecast from September 5th which aims to encapsulate the some of the details discussed. The forecast map shows the individual ensemble member forecast tracks on the left coloured by intensity of the 850 hPa vortex. Ellipses denote the likely forecast location at 24 hr intervals calculated as described in (**?**). The background contours show that the disturbance is over sea surface temperatures of around 27°C with all forecasts approaching warmer waters over the 120 hrs. The panels on the right of the figure, show the time series of each ensemble member for 4 variables, 850 hPa vorticity, 200-850 hPa vertical shear, total precipitable water and minimum mean sea level pressure (top to bottom respectively). These ensemble time-series are sorted per panel with respect to the 120 hr vortex strength. This graphic therefore shows that by 120 hrs there is reasonable spread across the ensembles with respect to low-level circulation. All members show intensification over the first 24-36 hrs but weaker members then level off and show weakening after 48 hours. The second panel displays the deep-layer shear for the ensemble members showing that throughout the forecast and for each ensemble member, shear remains less than 12-15 kts and typically is around 5-7.5 kts. As discussed in the analysis of this system, there was a large region of dry air west of the circulation and during this forecast time was also wrapping around the southwestern flank. The time series of TPW within 500 km of the system shows that generally the disturbance was in a region of approximately 52 mm of precipitable water however by forecast hour 48 the weakest members are starting to show a small decline in moisture around the system. This trend continues and by hour 72 the weakest members have declined to 45 mm while the strongest members have retained TPW values over 52 mm. The intensity evolution is reflected in the surface strength of the disturbance as well, with nearly all members showing an initial minimum in mslp around 1008 hPa, during the first 24-48 hours. After that initial intensification, the weaker members lose the surface pressure minimum with strong correlation to the circulation strength and moisture within the column. This plot identifies the variability in the forecasts and the sensitivity of the forecast intensity to the moisture associated with the disturbance, while showing that SSTs and deep layer shear remained relatively favourable for intensification.

5. Discussion

The analysis presented in this paper has documented the evolution of a strong AEW in the peak of the 2014 Atlantic hurricane season. As the wave approached the west African coast numerical and operational forecasts suggested a possibility of cyclogenesis occurring over the eastern Atlantic. In the following days however the system lacked deep organised convection as it interacted with a large region of dry air to the west and north of the circulation. In-situ observations were made by an unmanned global hawk aircraft operating during the HS3 field campaign, this provided both dropsondes and cloud physics lidar measurements of the system 2 days after leaving the coast.

During the AEWs' life over the African continent there were repeated diurnal bursts of convection associated with the strong jet-level vortex and likely contributing to the strength of the system (Berry and Thorncroft 2011, 2012). After leaving the continent however precipitation was substantially restricted in spatial extent to the northeast of the vortex. At this time, the dry air from the northwest created a strong gradient along the western edge of the circulation and was advected towards the south west extent of the circulation. Wave relative streamline analysis showed that during the first 2 days over the eastern Atlantic, there was a misalignment between the mid-level and low-level circulations. It is expected that as the circulation becomes misaligned either through the shallow vertical shear imposed by the AEJ that the vortex will then start to interact with the circulation above or below and rotate the column in a cyclonic manner (Jones 1995). Therefore although streamline analysis revealed closed circulation on isobaric layers, environmental air was shown in the analysis and dropsonde observations to be entraining above and/or below areas of closed circulation, limiting the convective ability of the trough.

Satellite and cloud physics lidar measurements of the dry air to the west of the disturbance revealed that there was relatively low amounts of dust throughout most of the dry air. Increased aerosol concentrations were observed along the gradient of the AEW circulation, suggesting that predominantly the dry air was likely low-level trade winds over the eastern Atlantic from mid-latitude subsidence as well as in-situ subsidence with a contribution of SAL associated with the circulation of the AEW. This highlights the potentially mixed origins of tropical dry air over the eastern Atlantic as suggested by Braun (2010).

Ensemble forecasts from the GFS model were used to assess the differences between developing and non-developing members of the same forecast as well as the systematic bias observed with the GFS over the eastern Atlantic for false alarms of tropical cyclogenesis (Halperin et al. 2013). Forecasts show that the track of the disturbance was relatively well forecast, however there was a consistent over intensification of the vortex as it transitioned over the coastal region. The over-intensification of the vortex was associated with a positive bias in θ_e throughout the lower troposphere and a persistent over forecast of precipitation around the vortex center. Autocorrelation of the ensemble characteristics showed that typically the 120 hr forecast was largely dependent on the characteristics of the vortex after 24-48 hours of the forecast. It is therefore suggested that given a marginal environment, low shear, warm ssts but dry surrounding conditions, strong disturbances can remain strong while being protected from the surrounding environment. As the vortex intensifies during the first 24-48 hours of the forecast, it becomes less sensitive to the environment and more dependent on the moisture within the trough and the boundary layer similar to that shown in (Torn and Cook 2013) . This allows continued convection to occur, thus maintaining the strength of the vortex and exacerbating the error in vortex intensity at longer lead times.

Further analysis of more non-developing events is therefore recommended to understand the processes limiting convection in strong vortices and the demise of the once favourable characteristics associated with such disturbances. Understanding the synoptic scale interaction between the circulation and the environment is also important in identifying situations where a small error in the short term forecast may be propagated downstream. The GFS has been shown to have a false alarm bias over the eastern Atlantic and the associated reanalysis (CFSR) has also been shown to have similar bias with respect to diabatic heating and low-level vorticity over the eastern Atlantic Janiga and Thorncroft (2012). This systematic overdevelopment of low-level vorticity in this region is suggested to over-protect the otherwise cold-core low-levels of the disturbance from the typically hostile environment to it's north and northwest. Further research of the false alarms in the forecast or reforecast model is recommended to identify whether false alarms in this region are typically due to the proposed lack of environmental interaction with unfavourable environmental conditions.

Acknowledgments. This research is supported in part by the NASA grant NNX10AU44G on the Hurricane Severe Storm Sentinel campaign and NOAA NA15NWS4680005. Analysis and plotting of data were conducted using the NCAR Command Language (Version 6.3.0) [Software]. (2014). Boulder, Colorado: UCAR/NCAR/CISL/VETS. http://dx.doi.org/10.5065/D6WD3XH5. The CFSR data used in this study were downloaded from the Research Data Archive (RDA), which is maintained by the Computational and Information Systems Laboratory (CISL) at the National Center for Atmospheric Research (NCAR) Saha et al. (2014). NCAR is sponsored by the National Science Foundation (NSF). The original CFSR data are available from the RDA (http://rda.ucar.edu) in dataset numbers ds093.0.

References

Arnault, J., and F. Roux, 2009: Case study of a developing African easterly wave during NAMMA: An energetic point of view. *J. Atmos. Sci.*, **66 (10)**, 2991–3020.

Arnault, J., and F. Roux, 2010: Comparison between two case studies of developing and nondeveloping African easterly waves during NAMMA and AMMA/SOP-3: absolute vertical vorticity budget. *Mon. Wea. Rev.*, **138 (4)**, 1420–1445.

Berry, G. J., and C. D. Thorncroft, 2005: Case study of an intense African easterly wave. *Mon. Wea. Rev.*, **133**, 752–766.

Berry, G. J., and C. D. Thorncroft, 2011: African Easterly Wave dynamics in a mesoscale numerical model: Part (ii): Synoptic modulation of convection. *Q. J. R. Meteorol. Soc.*

Berry, G. J., and C. D. Thorncroft, 2012: African Easterly Wave Dynamics in a Mesoscale Numerical Model: The Upscale Role of Convection. *J. Atmos. Sci.*, **69 (4)**, 1267–1283.

Bracken, W. E., and L. F. Bosart, 2000: The Role of Synoptic-Scale Flow during Tropical Cyclogenesis over the North Atlantic Ocean. *Mon. Wea. Rev.*, **128**, 353–276.

Brammer, A., and C. D. Thorncroft, 2015: Variability and Evolution of African Easterly Wave Structures and Their Relationship with Tropical Cyclogenesis over the Eastern Atlantic. *Mon. Wea. Rev.*, **143 (12)**, 4975–4995.

Brammer, A., and C. D. Thorncroft, 2017: Spatial and Temporal Variability of the Three-Dimensional Flow around African Easterly Waves. *Mon. Wea. Rev.*, **145 (7)**, 2879–2895.

Braun, S. A., 2010: Reevaluating the Role of the Saharan Air Layer in Atlantic Tropical Cyclogenesis and Evolution. *Mon. Wea. Rev.*, **138 (6)**, 2007–2037.

Braun, S. A., P. A. Newman, and G. M. Heymsfield, 2016: NASA's Hurricane and Severe Storm Sentinel (HS3) Investigation. *Bull. Amer. Meteor. Soc.*, **97 (11)**, 2085–2102.

Burpee, R., 1972: The origin and structure of easterly waves in the lower troposphere of North Africa. *J. Atmos. Sci.*, **29**, 77–90.

Burpee, R., 1974: Characteristics of North African easterly waves during the summers of 1968 and 1969. *J. Atmos. Sci.*, **31**, 1556–1570.

Carlson, T. N., 1969a: Some remarks on African disturbances and their progress over the tropical Atlantic. *Mon. Wea. Rev.*, **97 (10)**, 716–726.

Carlson, T. N., 1969b: Synoptic histories of three African disturbances that developed into Atlantic hurricanes. *Mon. Wea. Rev.*, **97 (3)**, 256–276.

Chiao, S., and G. S. Jenkins, 2010: Numerical Investigations on the Formation of Tropical Storm Debby during NAMMA-06. *Weather and Forecasting*, **25 (3)**, 866–884.

Dieng, A. L., S. M. Sall, A. Lazar, M. Leduc-Leballeur, and L. Eymard, 2014: Analysis of Strengthening and Dissipating Mesoscale Convective Systems Propagating off the West African Coast. *Mon. Wea. Rev.*, **142 (12)**, 4600–4623.

Dunion, J. P., and C. S. Velden, 2004: The Impact of the Saharan Air Layer on Atlantic Tropical Cyclone Activity. *Bull. Amer. Meteor. Soc.*, **85 (3)**, 353–365.

Dunkerton, T., M. Montgomery, and Z. Wang, 2009: Tropical cyclogenesis in a tropical wave critical layer: easterly waves. *Atmospheric Chemistry and Physics*, **9**, 5587–5646.

Erickson, C., 1963: An incipient hurricane near the West African coast. *Mon. Wea. Rev.*, **91 (2)**, 61–68.

Frank, N. L., 1970: ATLANTIC TROPICAL SYSTEMS OF 1969. *Mon. Wea. Rev.*, **98 (4)**, 307–314.

Fritz, C., and Z. Wang, 2013: A Numerical Study of the Impacts of Dry Air on Tropical Cyclone Formation: A Development Case and a Nondevelopment Case. *J. Atmos. Sci.*, **70 (1)**, 91–111.

Gray, W., 1968: Global view of the origin of tropical disturbances and storms. *Mon. Wea. Rev.*, **96 (10)**, 669–700.

Halperin, D. J., H. E. Fuelberg, R. E. Hart, J. H. Cossuth, P. Sura, and R. J. Pasch, 2013: An Evaluation of Tropical Cyclone Genesis Forecasts from Global Numerical Models. *Weather and Forecasting*, **28 (6)**, 1423–1445.

Hopsch, S. B., C. D. Thorncroft, and K. R. Tyle, 2010: Analysis of African Easterly Wave Structures and Their Role in Influencing Tropical Cyclogenesis. *Mon. Wea. Rev.*, **138 (4)**, 1399–1419.

Huffman, G. J., and Coauthors, 2007: The TRMM Multisatellite Precipitation Analysis (TMPA): Quasi-Global, Multiyear, Combined-Sensor Precipitation Estimates at Fine Scales. *J. Hydrometeor*, **8 (1)**, 38–55.

Janiga, M. A., and C. D. Thorncroft, 2012: Regional differences in the kinematic and thermodynamic structure of African easterly waves. *Q. J. R. Meteorol. Soc.*, **139 (675)**, 1598–1614.

Jones, S. C., 1995: The evolution of vortices in vertical shear. I: Initially barotropic vortices. *Q. J. R. Meteorol. Soc.*, **121 (524)**, 821–851.

Komaromi, W. A., and S. J. Majumdar, 2015: Ensemble-Based Error and Predictability Metrics Associated with Tropical Cyclogenesis. Part II: Wave-Relative Framework. *Mon. Wea. Rev.*, in press.

Landsea, C. W., 1993: A climatology of intense (or major) Atlantic hurricanes. *Mon. Wea. Rev.*, **121 (6)**, 1703–1713.

Leppert II, K. D., D. J. Cecil, and W. A. Petersen, 2013a: Relation Between Tropical Easterly Waves, Convection, and Tropical Cyclogenesis: A Lagrangian Perspective. *Mon. Wea. Rev.*, **141 (8)**, 2649–2668.

Leppert II, K. D., W. A. Petersen, and D. J. Cecil, 2013b: Electrically Active Convection in Tropical Easterly Waves and Implications for Tropical Cyclogenesis in the Atlantic and East Pacific. *Mon. Wea. Rev.*, **141 (2)**, 542–556.

Marchok, T. P., 2002: How the NCEP tropical cyclone tracker works. *25th Conf. on Hurricanes and Tropical Meteorology, San Diego, CA, Amer. Meteor. Soc.*, 21–22.

McBride, J. L., and R. Zehr, 1981: Observational analysis of tropical cyclone formation. Part II: Comparison of non-developing versus developing systems. *J. Atmos. Sci.*, **38 (6)**, 1132–1151.

Piersig, W., 1944: The cyclonic disturbances of the sub-tropical eastern North Atlantic. *Bull. Amer. Meteor. Soc.*, **25 (1)**.

Rios-Berrios, R., R. D. Torn, and C. A. Davis, 2016: An Ensemble Approach to Investigate Tropical Cyclone Intensification in Sheared Environments. Part I: Katia (2011). *J. Atmos. Sci.*, **73 (1)**, 71–93.

Saha, S., and Coauthors, 2010: The NCEP Climate Forecast System Reanalysis. *Bull. Amer. Meteor. Soc.*, **91 (8)**, 1015–1057.

Saha, S., and Coauthors, 2014: The NCEP Climate Forecast System Version 2. *J. Clim.*, **27 (6)**, 2185–2208.

Torn, R. D., 2010: Ensemble-Based Sensitivity Analysis Applied to African Easterly Waves. *Weather and Forecasting*, **25 (1)**, 61–78.

Torn, R. D., and D. Cook, 2013: The Role of Vortex and Environment Errors in Genesis Forecasts of Hurricanes Danielle and Karl (2010). *Mon. Wea. Rev.*, **141 (1)**, 232–251.

Ventrice, M. J., C. D. Thorncroft, and M. A. Janiga, 2012: Atlantic Tropical Cyclogenesis: A Three-Way Interaction between an African Easterly Wave, Diurnally Varying Convection, and a Convectively Coupled Atmospheric Kelvin Wave. *Mon. Wea. Rev.*, **140 (4)**, 1108–1124.

Wang, J., and Coauthors, 2010: Water vapor variability and comparisons in the subtropical Pacific from The Observing System Research and Predictability Experiment-Pacific Asian Regional Campaign (T-PARC) Driftsonde, Constellation Observing System for Meteorology, Ionosphere, and Climate (COSMIC), and reanalyses. *J. Geophys. Res.*, **115 (D21)**, D21 108.

Wang, Z., and I. Hankes, 2014: Characteristics of tropical easterly wave pouches during tropical cyclone formation. *Mon. Wea. Rev.*, **142 (2)**, 626–633.

Young, K., 2016: NCAR/EOL Technical Note Dropsonde Dry Bias . URL https://www.eol.ucar.edu/system/files/software/Aspen/Windows/W7/documents/Tech%20Note%20Dropsonde_Dry_Bias_20160527_v1.3.pdf.

6. Figures

LIST OF FIGURES

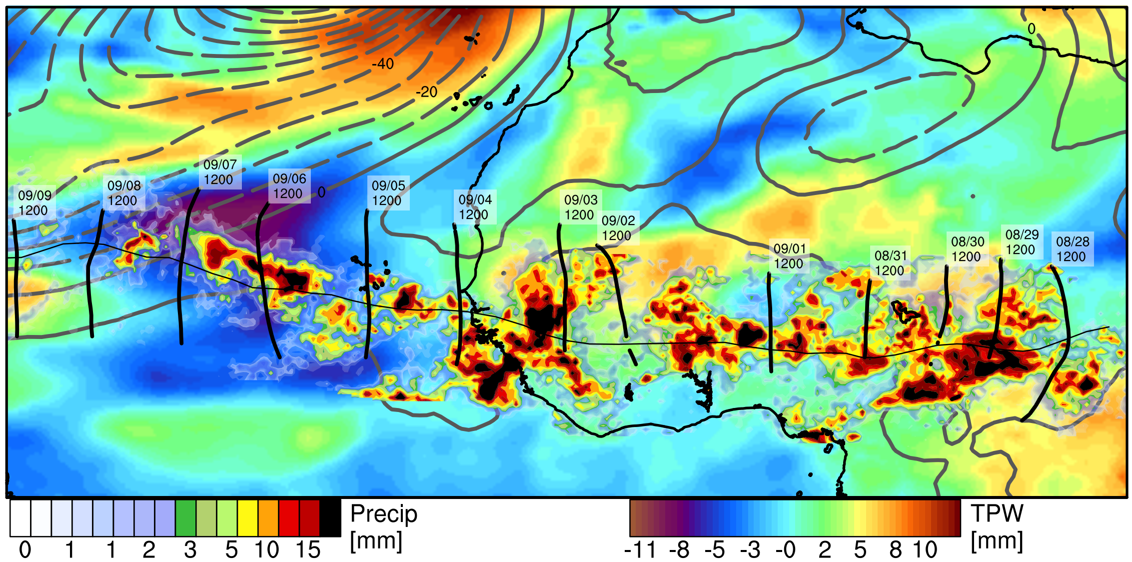

593 FIG. 1. Accumulated precipitation following pre-AL90 vortex (within 750 km), vertical black lines show objective trough axes every 24 hrs. Thin black line shows vortex track. Background shading and grey contours show daily mean total precipitable water and 300 hPa geopotential height for September 5th.

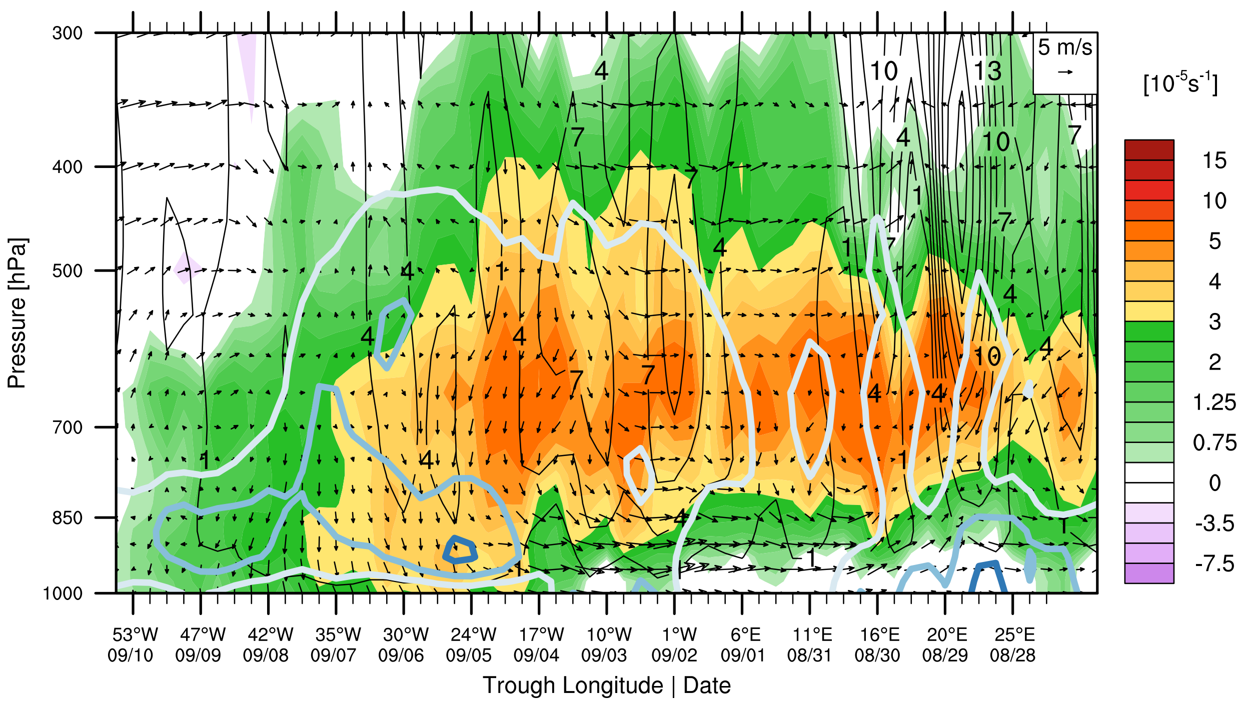

FIG. 2. Vertical profile evolution of relative vorticity (shading), specific humidity (contoured) and wave relative zonal and vertical wind (vectors) within 300 km of vortex center every 6 h.

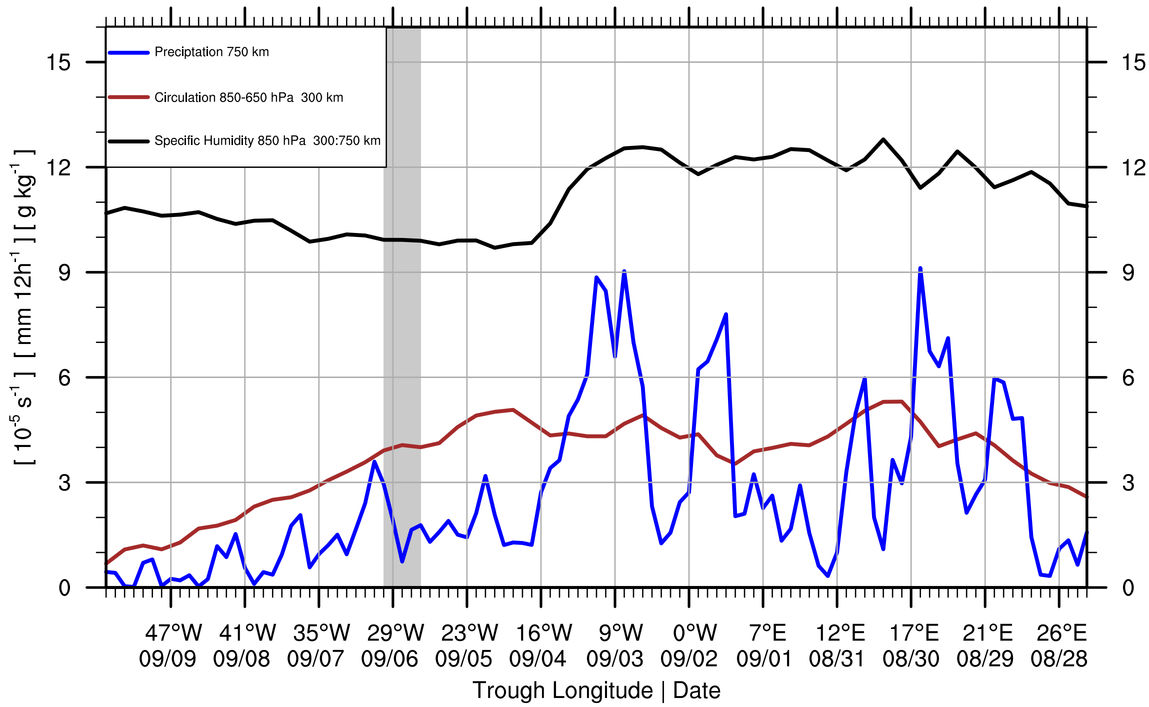

FIG. 3. Trough centric time-series of variables for specific humidity (850 hPa) averaged over an annulus of 300-750 km from the vortex center, circulation (850 hPa; radius of 300 km) and TRMM 3b42 precipitation averaged over a radius of 750 km.

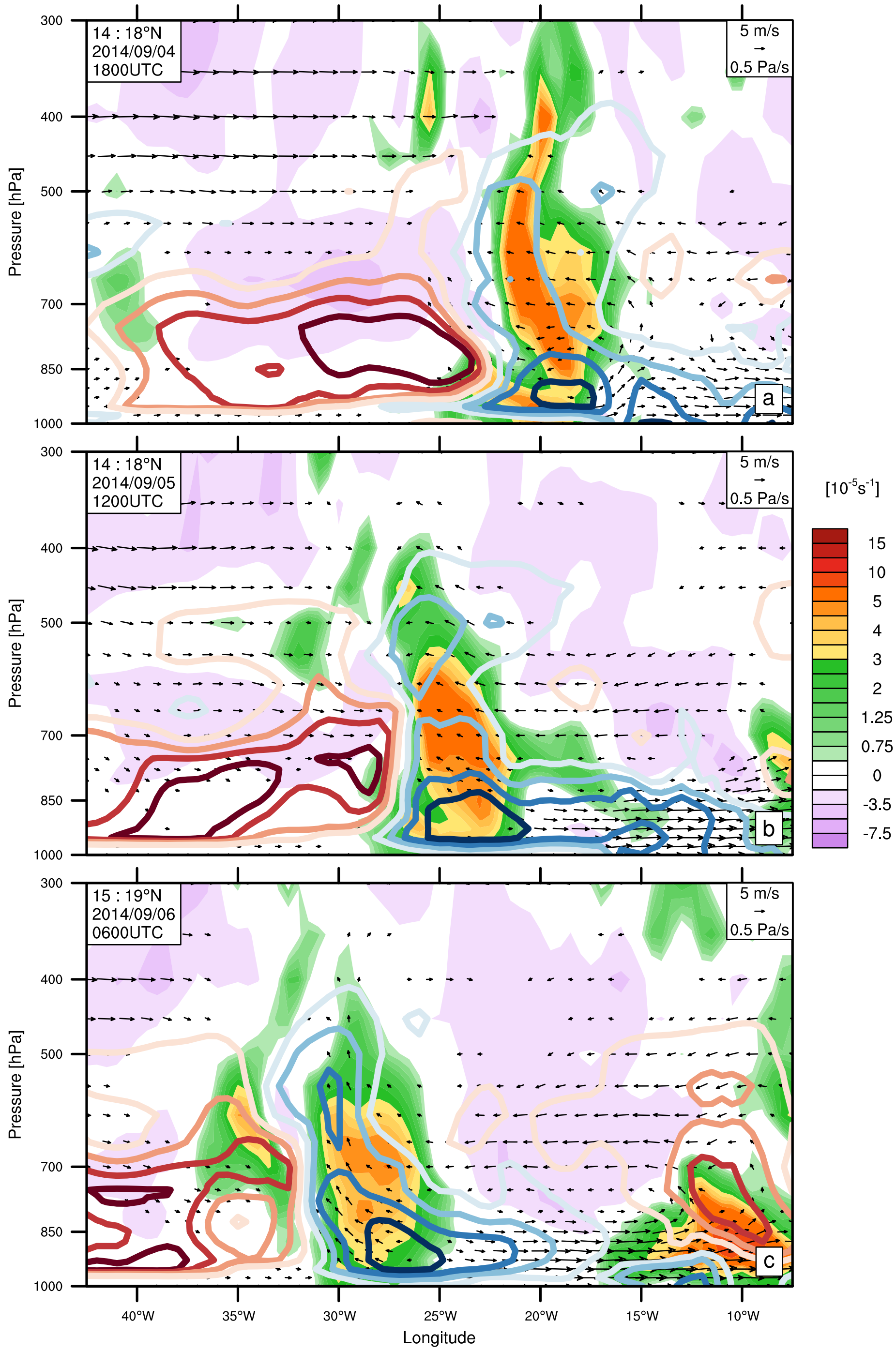

601 FIG. 4. Vertical cross sections of relative vorticity (shading), specific humidity (contoured) and wave relative
602 zonal and vertical wind (vectors) for September 4th 1800UTC (a), 5th 1200UTC (b) and 6th 0600UTC (c).

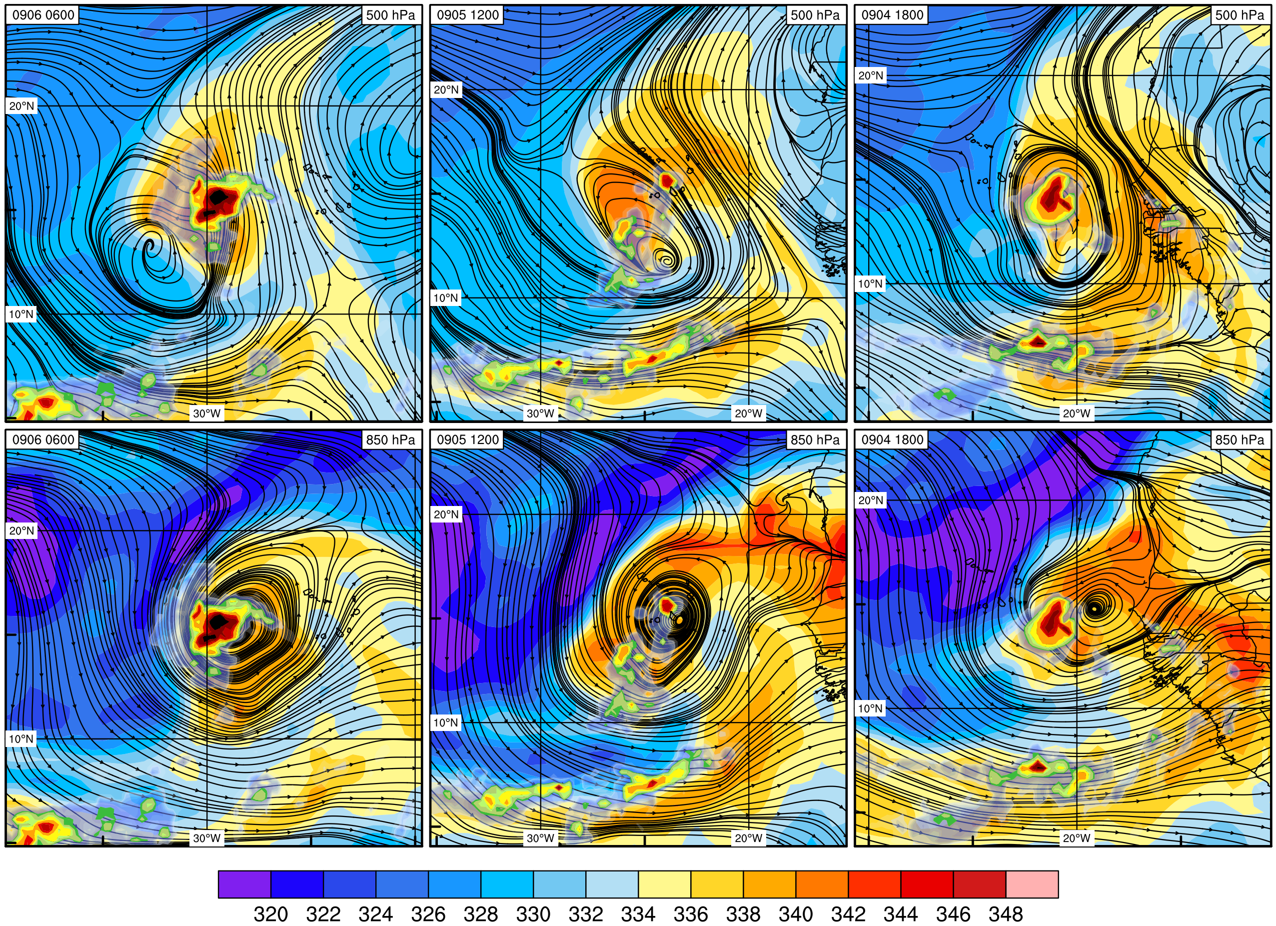

FIG. 5. Equivalent Potential Temperature (background shading), wave relative streamlines for 500 and 850 hPa, and overlaid on both levels is TRMM 3B42 precipitation contoured as Fig. 1. Maps show data for September 4th 1800UTC (left), 5th 1200UTC (middle) and 6th 0600UTC (right).

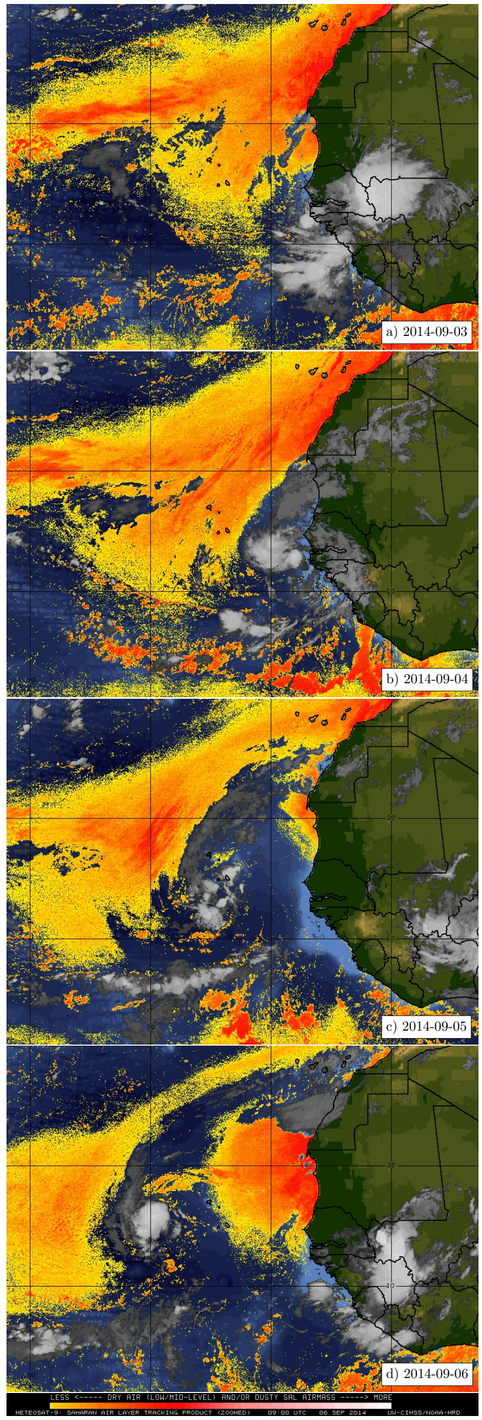

606 FIG. 6. Meteosat-9 IR clouds overlayed with the split-window Saharan Air Layer Tracking product generated by CIMSS, note the algorithm is sensitive to both dry and/or dusty airmass in the lower troposphere. (Dunion and Velden 2004)

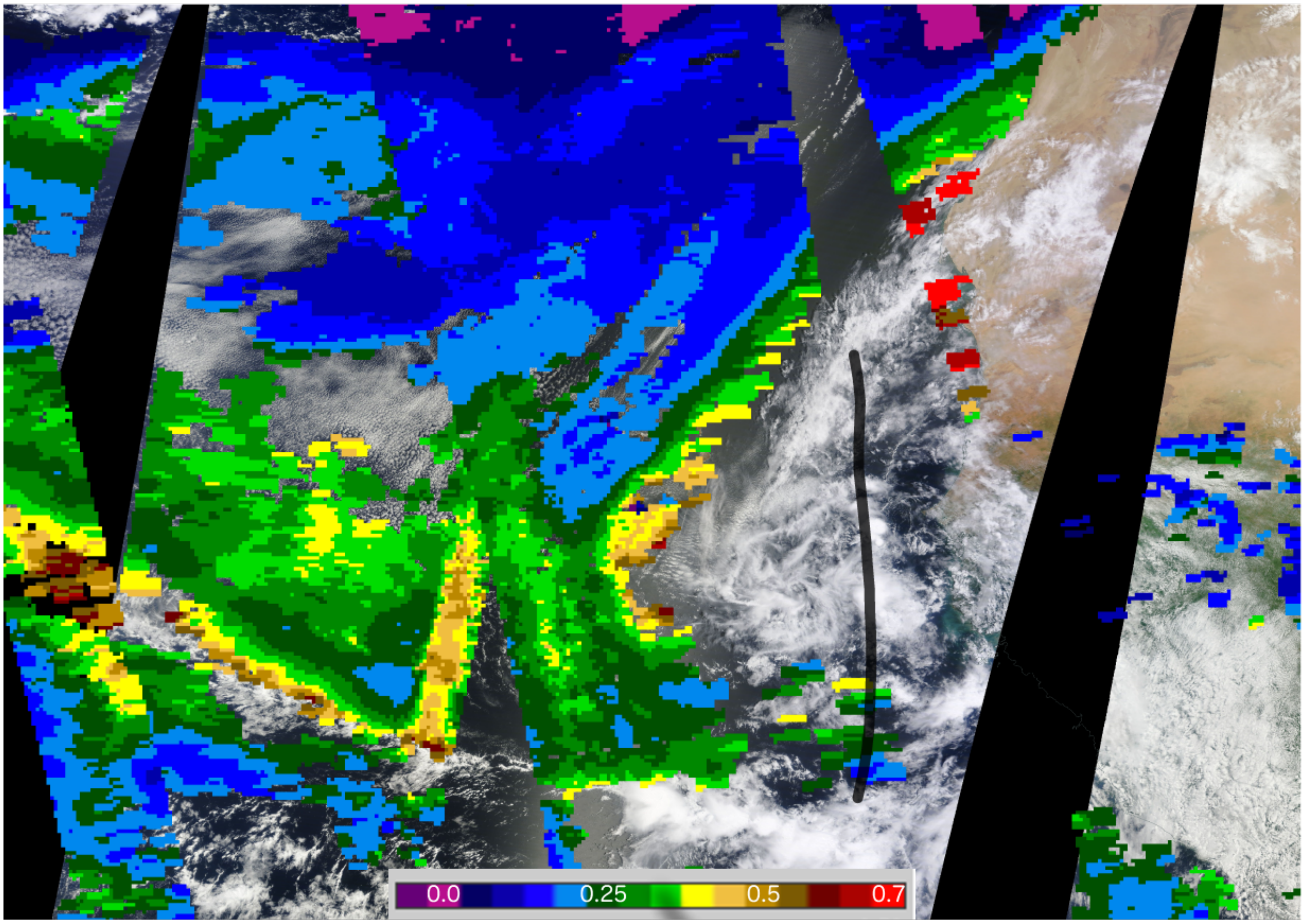

FIG. 7. Aerosol optical depth and corrected reflectance for September 4th 2014 merged from Terra and Aqua on MODIS. Image downloaded from NASA worldview website. Black trough line overlaid manually using 1200UTC location.

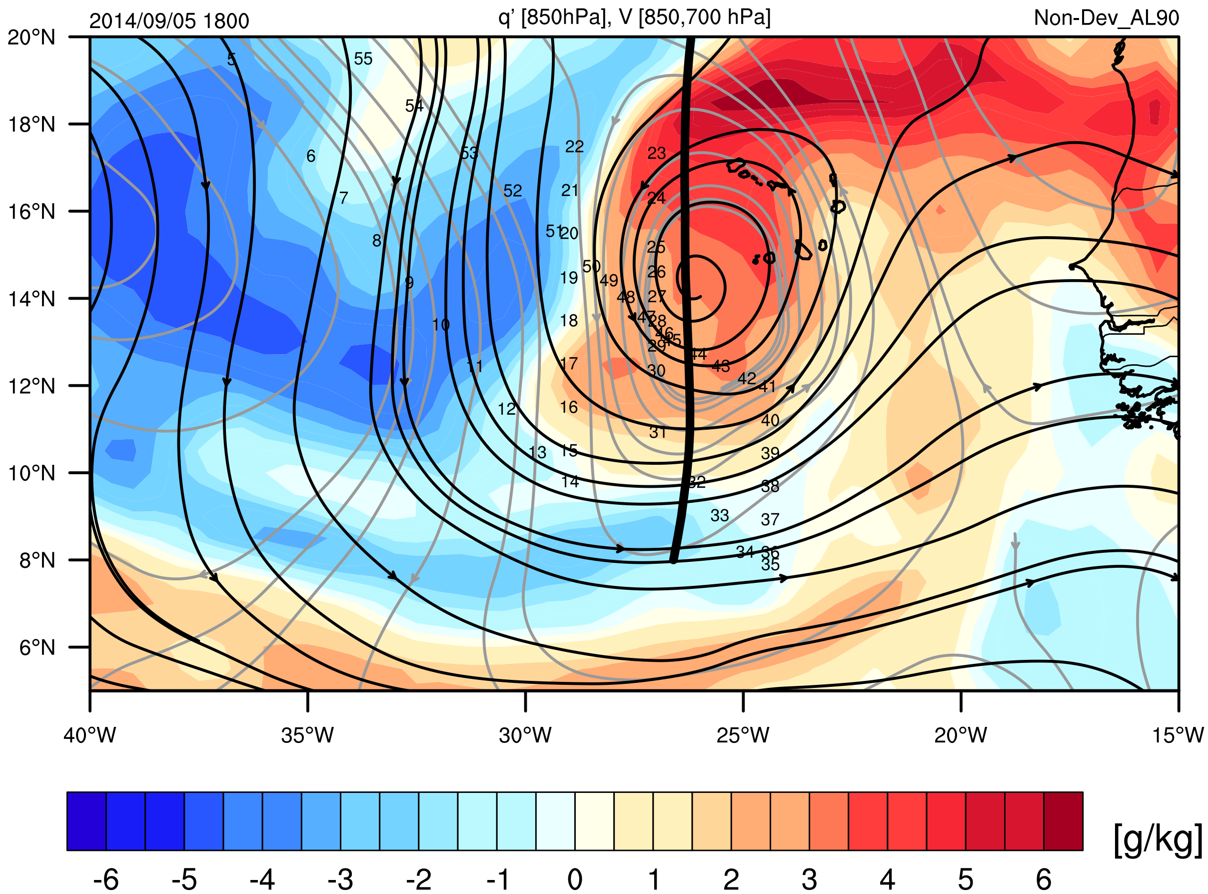

612 FIG. 8. Location of Dropsondes overlaid on anomalous specific humidity at 850 hPa and trough relative
613 streamlines at 850 hPa (Black) and 700 hPa (Grey). Humidity and wind vectors taken from CFSR at 1800UTC
614 approximately when drop 5 was released for reference drop 14 was released at 2114UTC.

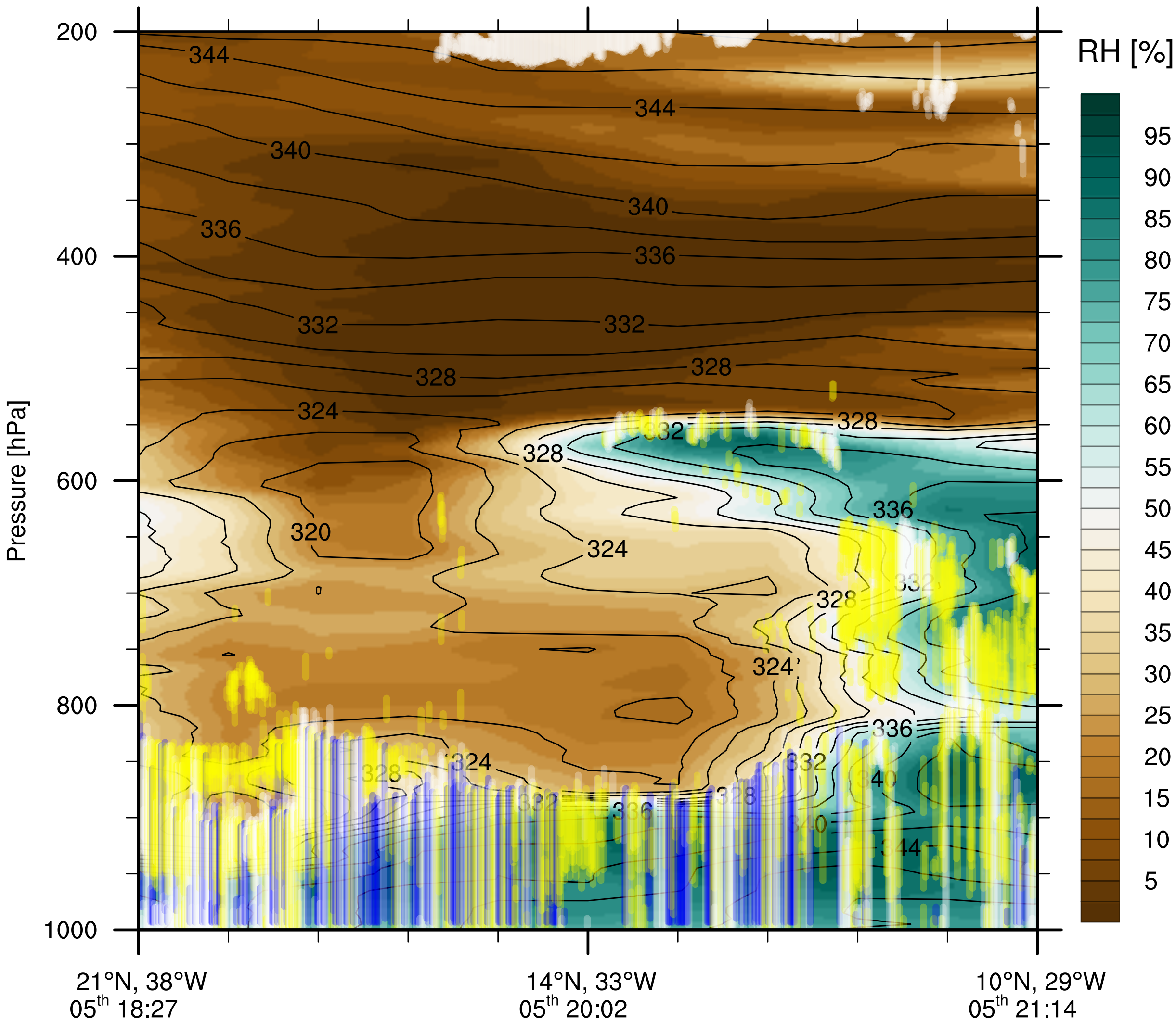

FIG. 9. Cross section of relative humidity (shading), equivalent potential temperature (contour lines) and overlaid layer detection as measured by CPL. CPL detects up to 8 layers of three types; cloud (white), elevated aerosol (yellow) and boundary layer (blue).

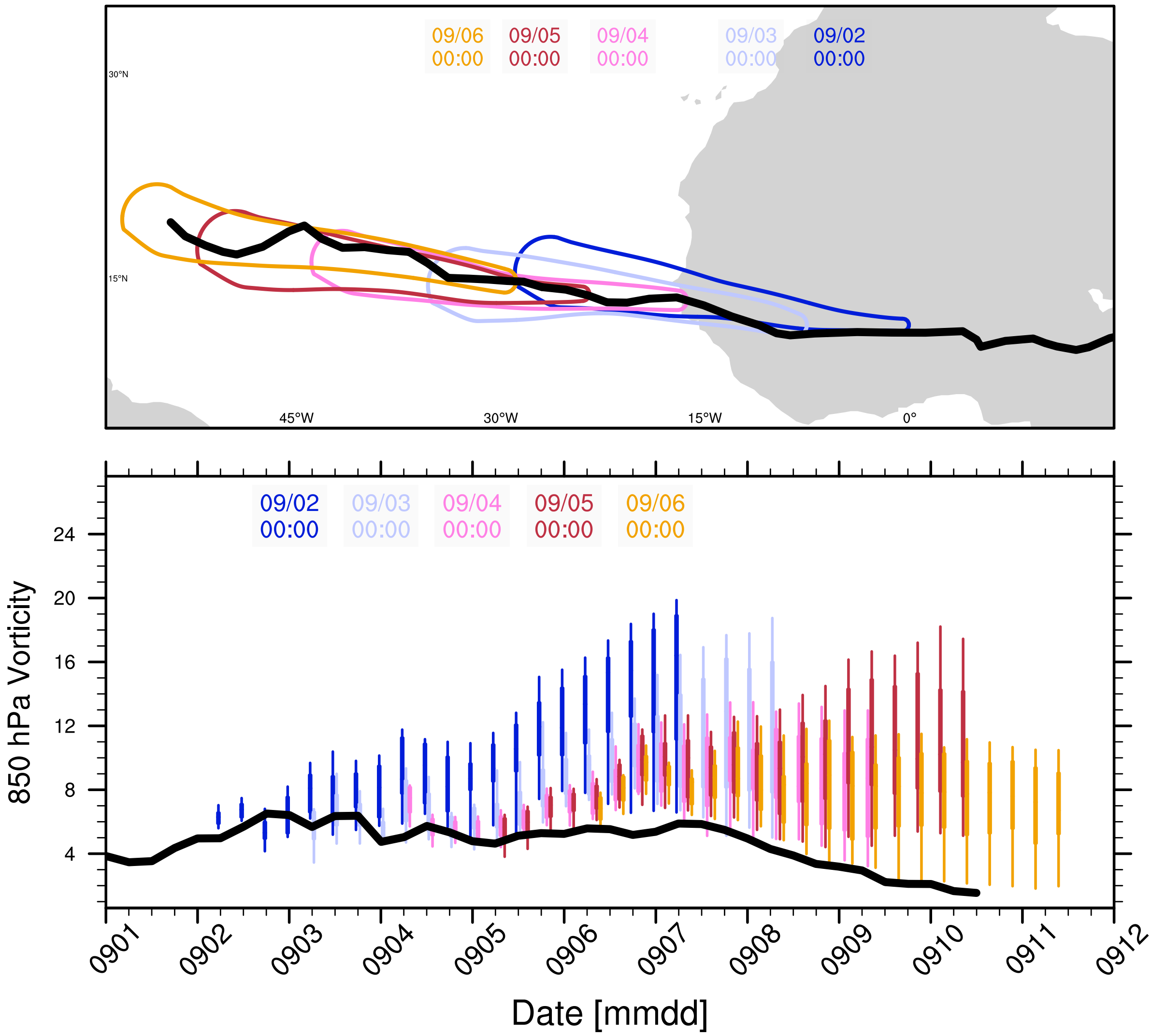

FIG. 10. Ensemble forecasts from the operational GEFS during the coastal transition of AL90. a) displays 120-hr forecast cones, created using the ensemble mean track $\pm$ 1σ of across track spread. b) distribution of the ensemble forecast 850 hPa vorticity (averaged over 250 km radius). For each plot, the colors represent each days 00UTC forecast.

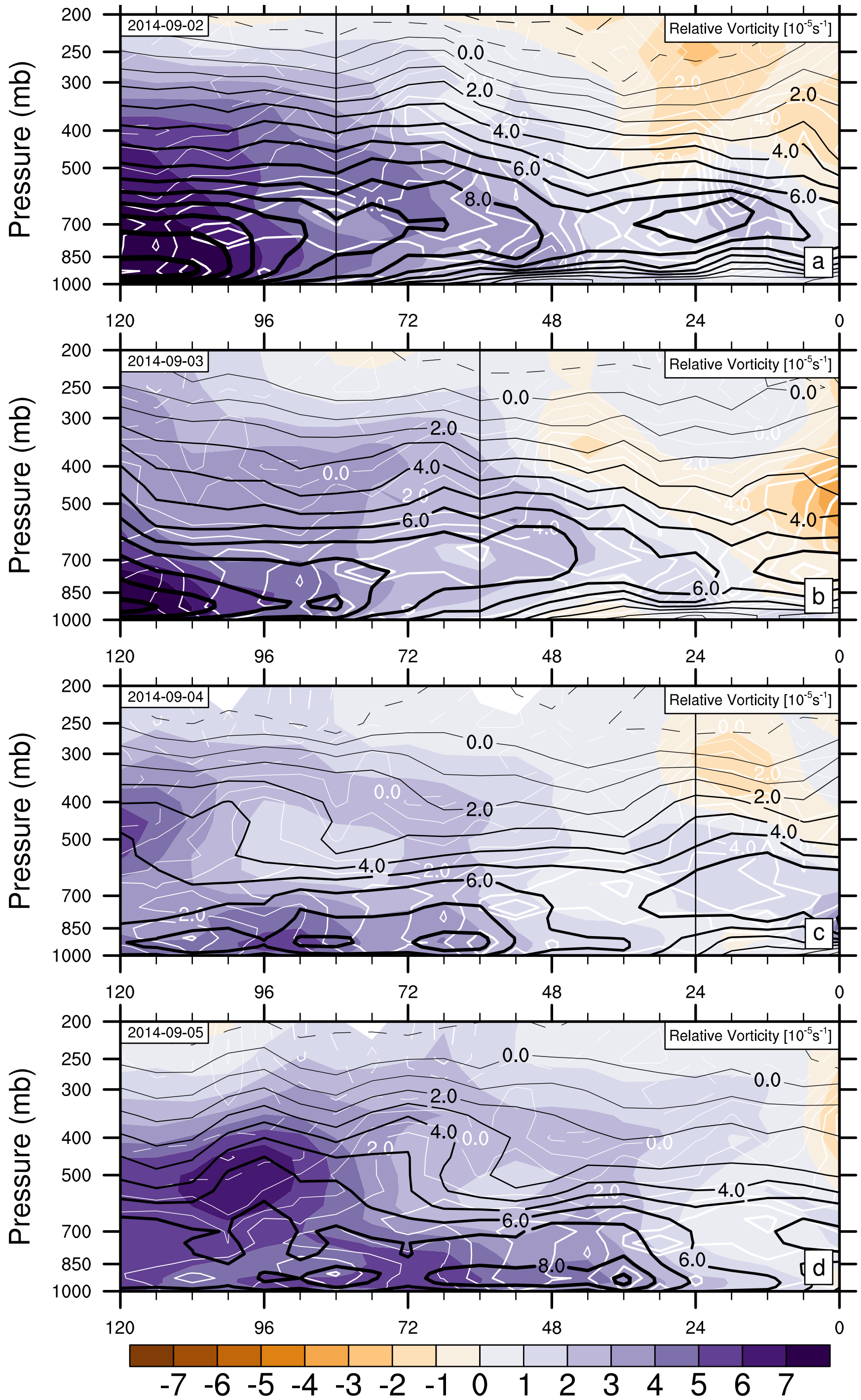

FIG. 11. Forecast evolution of the vertical profile of relative vorticity around the analysis (white contours) and ensemble mean (black contours) vortex. The ensemble mean error is shown in shading. Forecast hour increases from right to left, as the trough moves east to west. The vertical black line denotes the trough passage over the coast.

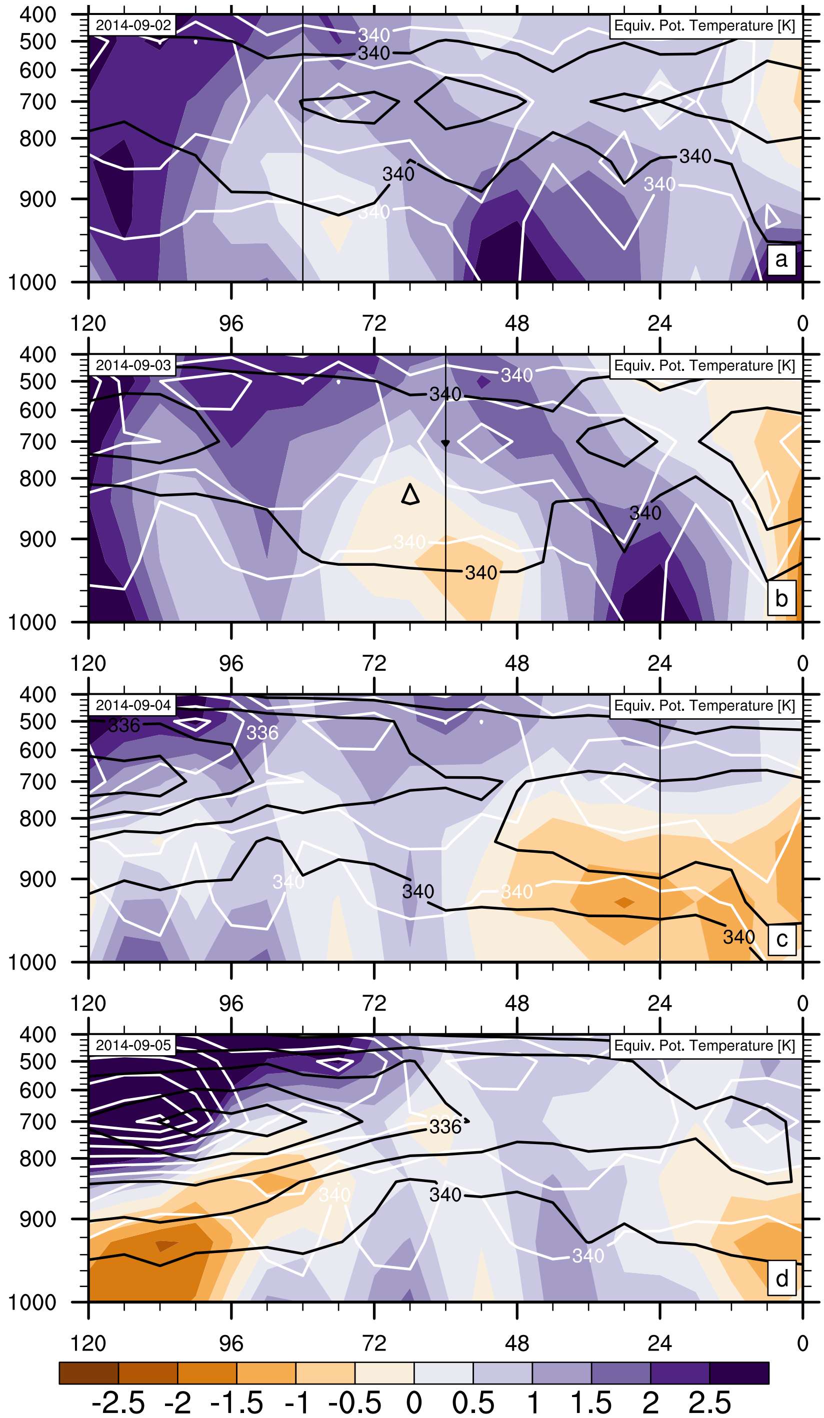

FIG. 12. Forecast evolution of the vertical profile of θ_e around the analysis (white contours) and ensemble mean (black contours) vortex. The ensemble mean error is shown in shading. Forecast hour increases from right to left, as the trough moves east to west. The vertical black line denotes the trough passage over the coast.

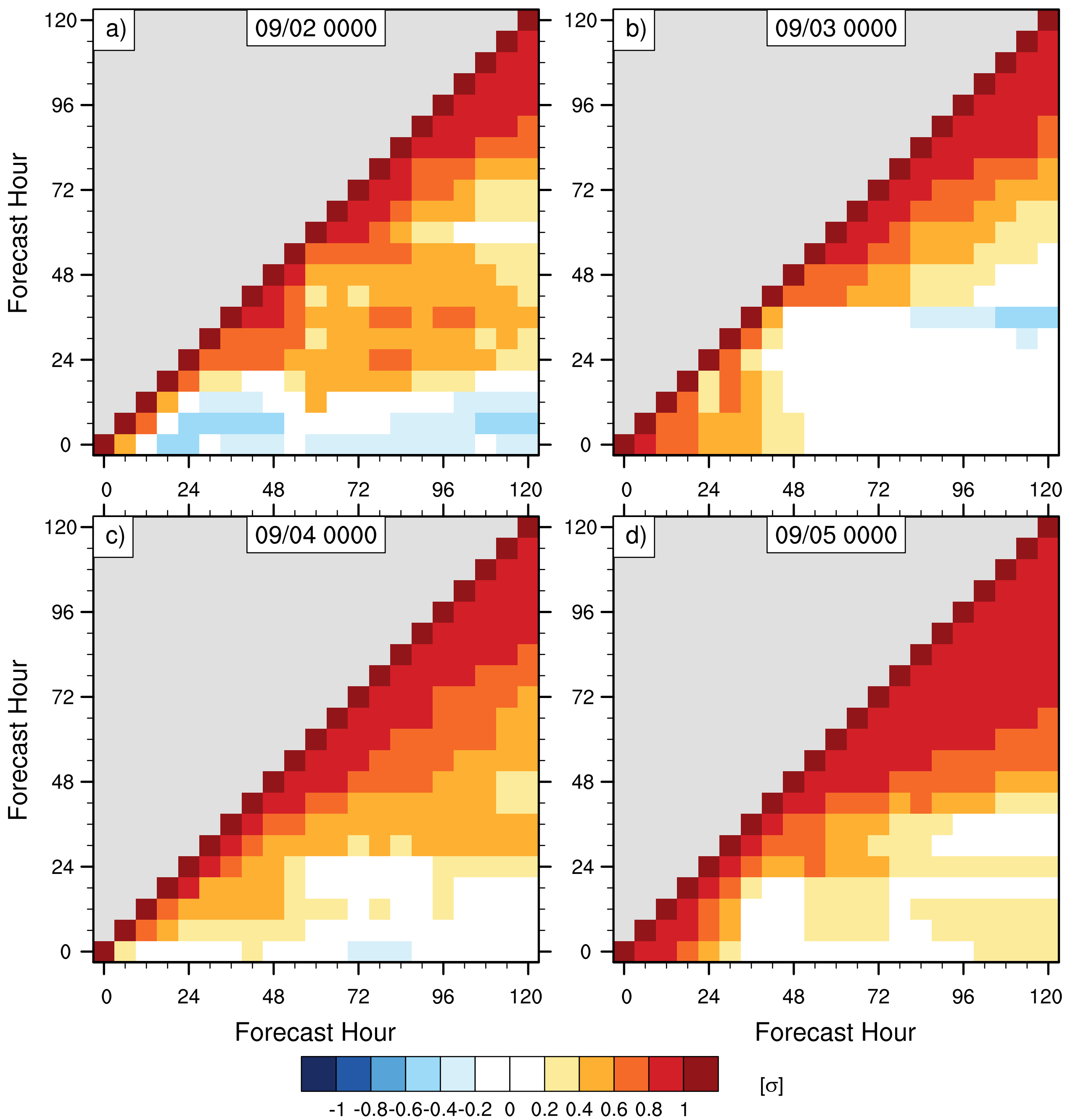

629 FIG. 13. Correlation between the intensity of the 850hPa 300 km circulation around ensemble forecast troughs

630 with intensity of the circulation at subsequent lead times. Panels show different initialisation times.

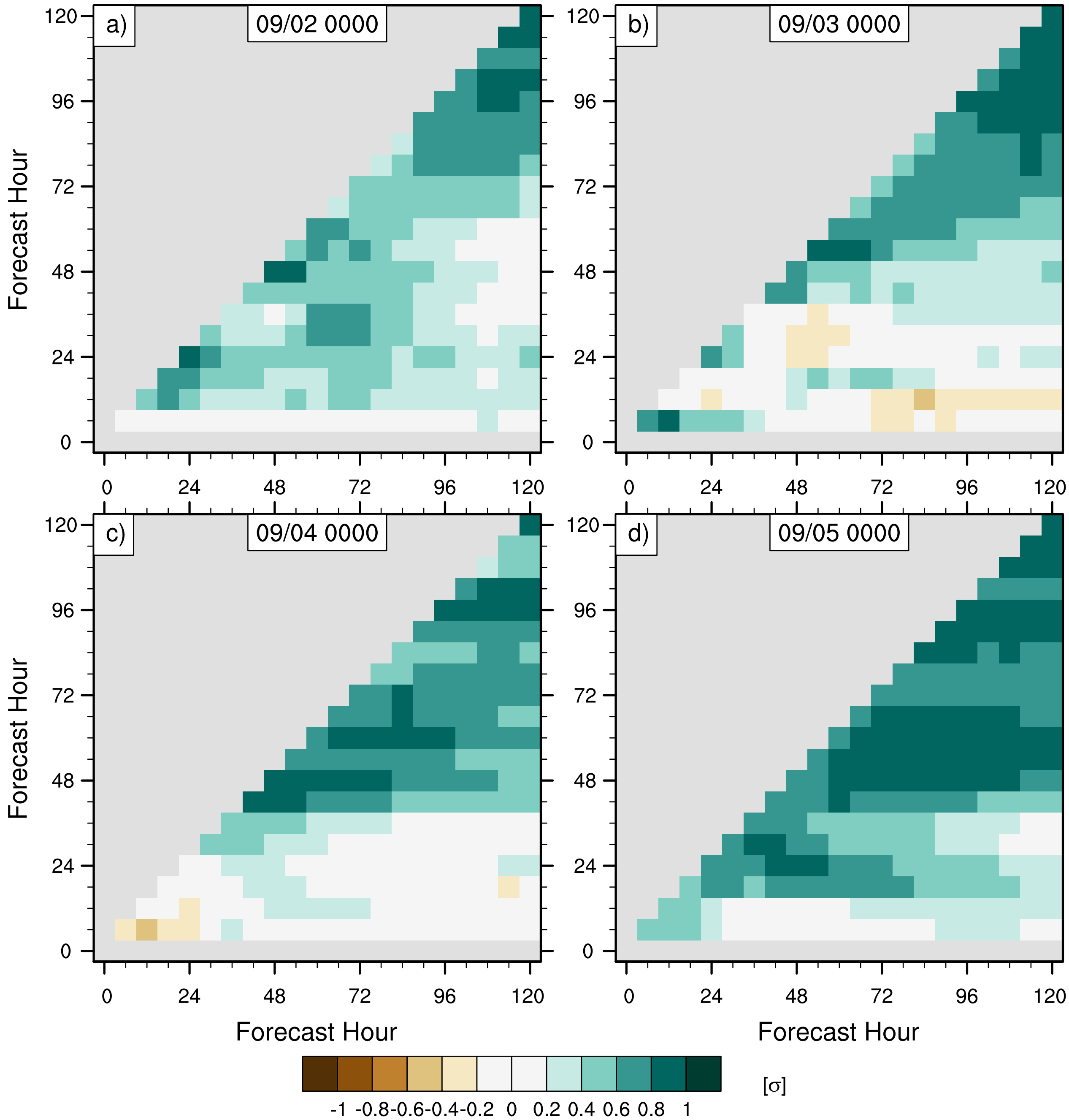

FIG. 14. Correlation between the precipitation within 300 km of ensemble forecast vortex with intensity of the 850 hPa 300 km circulation at subsequent lead times. Panels show different initialisation times.

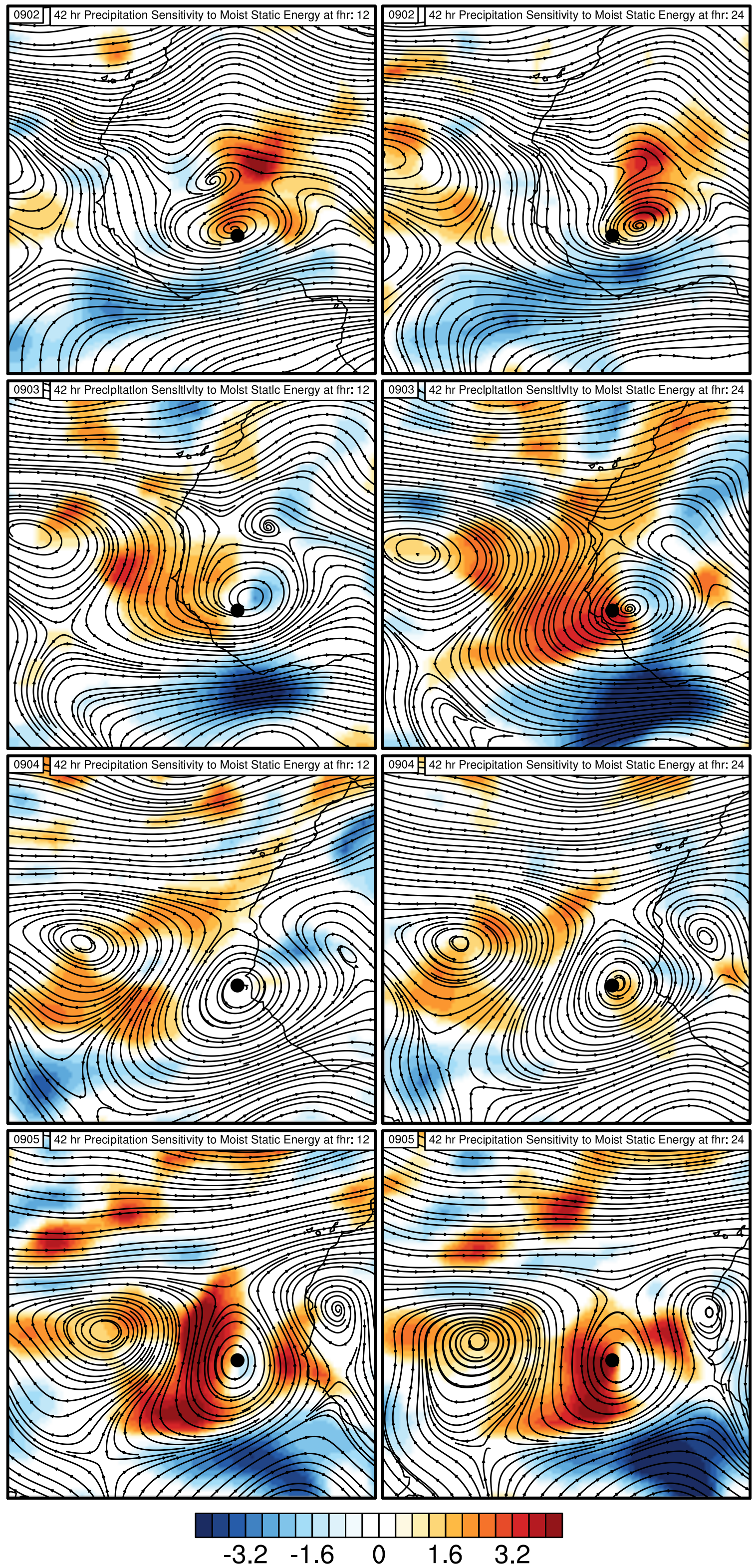

FIG. 15. Trough relative streamlines layer averaged between 900-700 hPa. Shading shows sign and significance of the ensemble based 42 hr precipitation forecast sensitivity to layer average moist static energy. Positive shading denotes increased moist static energy at that location is significantly correlated to increased precipitation in the trough at hour 42.

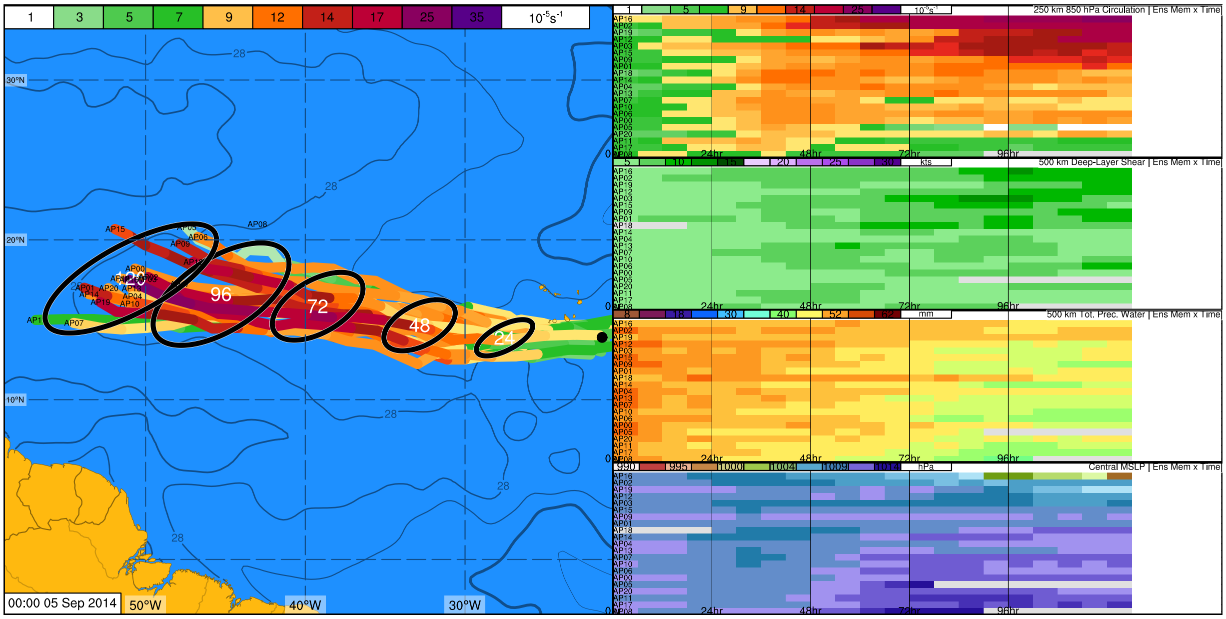

FIG. 16. GEFS ensemble forecast for AL90 initialized 0000UTC September 5th. Left shows tracks for each ensemble member colored by 850 hPa circulation strength. Ellipses represent uncertainty around forecast location at each 24 hr interval. Background contours show SST (1°C intervals, 26°C thick contour). Plots on right show colored time-series for each ensemble member stacked vertically and sorted vertically by maximum forecast circulation over the 120 hrs. a) Forecast 850 hPa circulation (250 km radius average); b) Deep-layer vertical shear (averaged over 500km radius from center); c) Total precipitable water (averaged over 500km radius); d) minimum central mean sea-level pressure (within 300km of center).